6

Schwinger–Dyson equations in the pinch technique framework

In this chapter, we provide a detailed demonstration of how the application of the PT algorithm at the level of the conventional Schwinger–Dyson series leads to a new, modified Schwinger–Dyson equation (SDE) for the gluon propagator endowed with very special truncation properties. In particular, because of the QED-like Ward identities from the fully dressed Green's functions entering into the gluon SDE, the transversality of the gluon self-energy is guaranteed at each level of the dressed-loop expansion. This result constitutes one of the main objectives of the PT program, namely, the device of a gauge-invariant truncation scheme for the equations governing the nonperturbative dynamics of non-Abelian Green's functions.

Of course, like any propagator SDE, this equation depends on the full three- and four-point gluon vertices, and these in turn depend on infinitely many other Green's functions. We have suggested, in the last chapter, how to truncate the SDE for the PT propagator by using the gauge technique to approximate the three- and four-point PT Green's functions as functionals only of the PT proper self-energy, while maintaining the exact Ward identities demanded by the PT. This approximation can only be useful in the infrared; the gauge technique PT Green's functions clearly fail to be exact at large momenta (although this failure is quantitative, not qualitative, so it should not change the fundamental findings from PT SDEs, except in the numerics).

For the purposes of this book, it would be too much to study thoroughly all the ramifications of combining the gauge technique, which, in its most general form, is quite complicated, with the pinch technique in the all-order SDEs. In fact, this has not yet been done. The emphasis in this chapter will be on the SDEs themselves, not on how to make approximations to them. However, we will present some applications in which a relatively simple version of the gauge technique provides the necessary structure for maintaining gauge invariance and obtaining massive (infrared finite) solutions.

As far as the fundamental underlying dynamics are concerned, there is no qualitative difference between the all-order SDEs presented here and the simple one-loop equations of Chapters 1 and 2: infrared slavery demands the generation of a

114

dynamical gluon mass of about half a GeV. Before going into detail, we really should ask whether it is worth it – is there any solid evidence that the gluon does have a mass? Of course, this cannot be a direct experimental finding because gluons are screened out of physical existence as isolated particles. But for QCD theorists, lattice simulations are the ideal laboratory, and so we begin with summarizing the lattice evidence for the gluon mass. These simulations are done in Euclidean space, which leads us to the following notational changes. We will derive the SDEs in Minkowski space, as we have used so far. But beginning with Section 6.5 and through the rest of the chapter, we will work in Euclidean space, with metric $\delta_{\mu\nu}$, for ease of comparison with lattice data.

6.1 Lattice studies of gluon mass generation

The experimental laboratory for validation of PT results is the computer, and the experiments are simulations. In this case, we ask what simulations of gluon propagators say about the gluon mass. A large number of such simulations have been done by a number of different groups [1, 2, 3, 4, 5, 6, 7, 8, 9, 10, 11, 12, 13, 14, 15, 16, 17, 18, 19, 20, 21]. All these simulations, for technical reasons, are gauge fixed to a Landau gauge[1] rather than using the background-field Feynman gauge, which would then yield the PT propagator. The Landau gauge propagator is not gauge invariant, but it has one crucial feature: if the gluon has a mass, the propagator will be finite and nonvanishing at zero momentum – because it would have a zero-momentum singularity if the gluon were massless. This evidence for a massive gluon is found in all lattice simulations of the Landau-gauge gluon propagator cited earlier.

If it were possible to extend the Landau-gauge propagator to the region of timelike momenta, the position of the pole found in the propagator would be gauge invariant and yield the gluon mass. Such an extrapolation is risky, and neither we nor the simulations' workers have done this systematically and compared all the various results. However, to our eyes, all the propagator results are quite similar and presumably yield gluon masses in a fairly narrow range, and when the authors do give approximate mass values, they all cluster around 500–700 MeV. One group [1, 2] has attempted an extrapolation, making use of the functional form of the older PT propagator found in the first attempt [23] at calculating the PT propagator, which yields a very good fit for a gluon mass of around 600 MeV. It is not clear why a PT propagator should fit the simulated Landau-gauge propagator so closely. This issue needs lattice simulations in a background-field Feynman gauge, which do not yet exist. Figure 6.1 shows recent, and typical, lattice results for the gluon

---

[1] A Landau gauge has Gribov ambiguities [22]; various simulation groups take various approaches to resolving this issue, as detailed in specific papers. The upshot is that all groups claim that their results are more or less free of Gribov ambiguity problems.
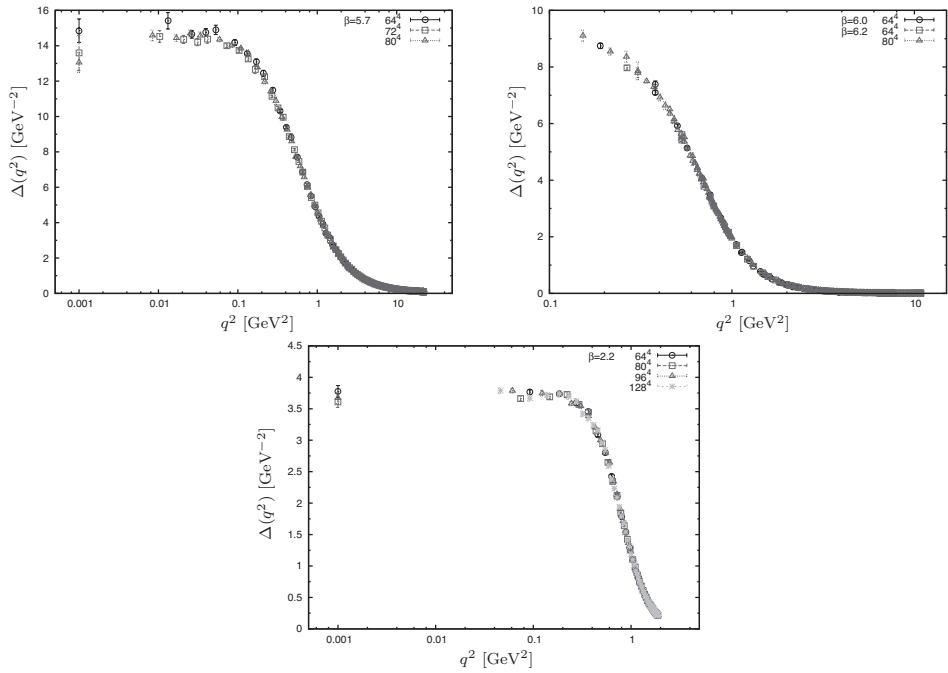
Figure 6.1. Lattice results for the gluon propagator from three different lattice groups. (*Upper left*) Bare lattice $SU(3)$ gluon propagator (data from Bogolubsky et al. [15]). (*Upper right*) $SU(3)$ gluon propagator renormalized at 3 GeV (data from Oliveira and Silva [11]). (*Lower left*) Bare $SU(2)$ propagator (data from Cucchieri and Mendes [19]).
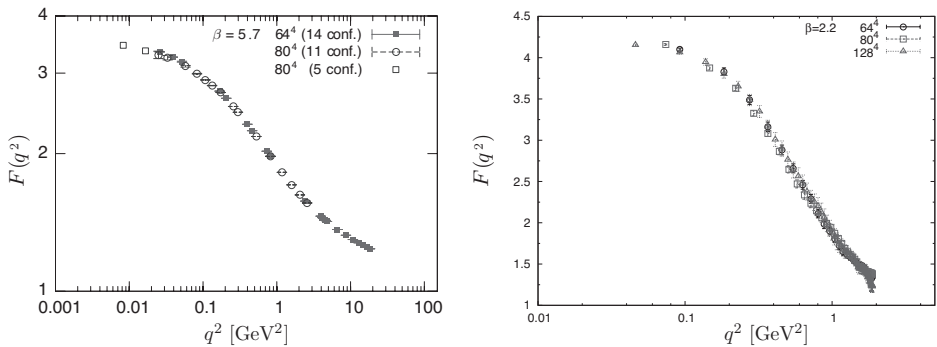

Figure 6.2. (*Left*) Bare lattice $SU(3)$ ghost dressing function. Reprinted with permission from I. L. Bogolubsky, E. M. Ilgenfritz, M. Muller-Preussker, and A. Sternbeck, *Phys. Lett.* **B676** (2009) 69; © 2009 by Elsevier. (*Right*) Bare $SU(2)$ ghost dressing function (data from Cucchieri and Mendes [19]).

propagator $\Delta(q^2)$ obtained by three different lattice groups [15, 19, 11]; Figure 6.2 shows the ghost propagator dressing function $F(q^2)$ (defined as the product of q^2 times the ghost propagator).

Note that in this figure, positive q^2 means a Euclidean (spacelike) momentum. The dressed gluon propagator is *finite* at zero momentum, indicating a gluon mass; if the mass were zero, the zero-momentum value would be infinite. Similarly, the ghost dressing function approaches a finite value at zero momentum. Both these properties will be found in the solutions to the PT SDEs of this chapter. We now go on to the meat of this chapter: the gauge-invariant PT SDEs and gluon mass generation.

6.2 The need for a gauge-invariant truncation scheme for the Schwinger–Dyson equations of NAGTs

The SDEs provide a formal framework for tackling physics problems requiring a nonperturbative treatment. Given that the SDEs constitute an infinite system of coupled nonlinear integral equations for all Green's functions of the theory, their practical usefulness hinges crucially on one's ability to devise a self-consistent truncation scheme that would select a tractable subset of these equations without compromising the physics one hopes to describe.

In Abelian gauge theories, the Green's functions satisfy naive Ward identities: the all-order generalization of a tree-level Ward identity is obtained simply by replacing the Green's functions appearing in it by their all-order expressions. In general, as we have seen, this is not true in non-Abelian gauge theories, where the Ward identities are modified nontrivially beyond tree level and are replaced by more complicated expressions known as Slavnov–Taylor identities: in addition to the original Green's functions appearing at tree level, they involve various composite *ghost operators*.

To appreciate why the Ward identities are instrumental for the consistent truncation of the SDEs, whereas the Slavnov–Taylor identities complicate it, let us first consider how nicely things work in an Abelian case, namely, *scalar* QED (photon), and then turn to the complications encountered in QCD (gluon).

Local gauge invariance (BRST in the case of the gluon) forces $\Pi_{\alpha\nu}(q)$ (photon and gluon alike) to satisfy the fundamental transversality relation

$$q^\alpha \Pi_{\alpha\beta}(q) = 0, \tag{6.1}$$

both perturbatively (to all orders) and nonperturbatively. The SDE governing $\Pi_{\alpha\beta}(q)$ in scalar QED is shown in Figure 6.3. The main question we want to address is the following: can one truncate the right-hand side (rhs) of Figure 6.3, i.e., eliminate some of the graphs, without compromising the transversality of $\Pi_{\alpha\beta}(q)$? The answer is shown already in Figure 6.3: the two blocks of graphs
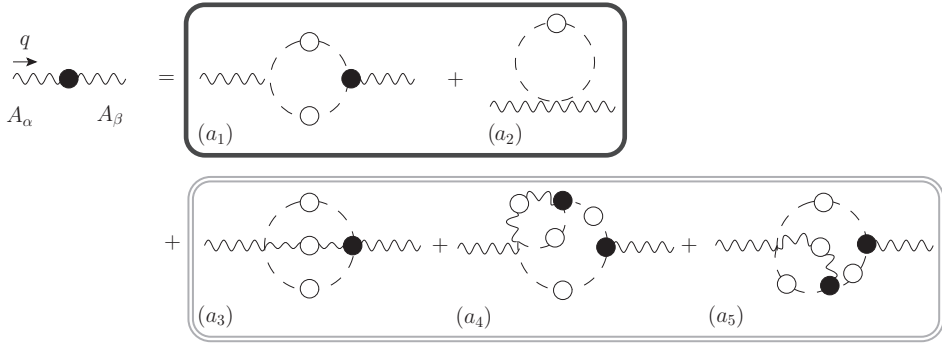
Figure 6.3. The SDE for the photon self-energy in scalar QED. The two boxes enclose a gauge-invariant subset of diagrams.

$[(a_1) + (a_2)]$ and $[(a_3) + (a_4) + (a_5)]$ are *individually transverse*, i.e.,

$$q^\alpha \sum_{i=1}^{2} (a_i)_{\alpha\beta} = 0 \qquad q^\alpha \sum_{i=3}^{5} (a_i)_{\alpha\beta} = 0. \tag{6.2}$$

The reason for this special property is precisely the Ward identities satisfied by the full vertices appearing on the rhs of the SDE; for example, the first block is transverse simply because the *full* photon-scalar vertex Γ_μ (black blob in (a_1)) satisfies the Ward identity:

$$q^\alpha \Gamma_\alpha = e[\mathcal{D}^{-1}(k+q) - \mathcal{D}^{-1}(k)], \tag{6.3}$$

where $\mathcal{D}(q)$ is the *full* propagator of the charged scalar. A similar Ward identity relating the four-vertex with a linear combination of Γ_α forces the transversality of the second block in Figure 6.3. Thus, owing to the simple Ward identities satisfied by the vertices appearing on the SDE for $\Pi_{\alpha\beta}(q)$, one may omit the second block of graphs and still maintain the transversality of the answer intact, i.e., the approximate $\Pi_{\alpha\beta}(q)$ obtained after this truncation satisfies Eq. (6.1).

Let us now turn to the *conventional* SDE for the gluon self-energy, in the R_ξ gauges, given in Figure 6.4. Clearly, by virtue of Eq. (6.1), we must have

$$q^\alpha \sum_{i=1}^{5} (a_i)_{\alpha\beta} = 0. \tag{6.4}$$

However, unlike the Abelian example, the diagrammatic verification of Eq. (6.4), i.e., through contraction of the individual graphs by q^α, is very difficult, essentially because of the complicated Slavnov–Taylor identities satisfied by the vertices involved. For example, the full three-gluon vertex $\Gamma_{\alpha\mu\nu}(q, k_1, k_2)$ satisfies the
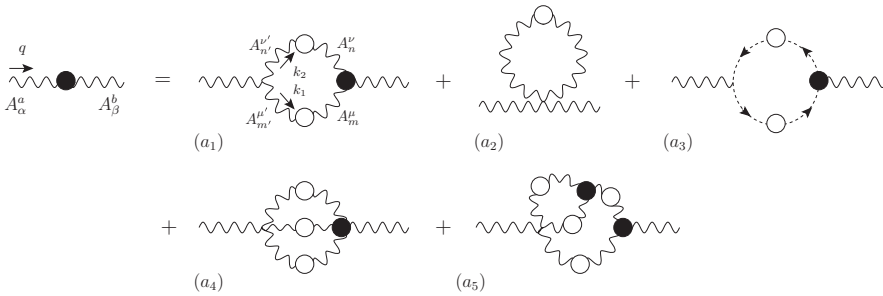
Figure 6.4. Schwinger-Dyson equation satisfied by the gluon self-energy $-\Gamma_{AA}$. The symmetry factors of the diagrams are $s(a_1, a_2, a_5) = 1/2$, $s(a_3, a_6) = -1$, and $s(a_4) = 1/6$.

Slavnov–Taylor identity of Eq. (1.89). In addition, some of the pertinent Slavnov–Taylor identities are either too complicated, such as that of the conventional four-gluon vertex, or cannot be cast in a particularly convenient form, such as that of the conventional gluon-ghost vertex. The main practical consequence of this is that one cannot truncate the rhs of Figure 6.4 in any obvious way without violating the transversality of the resulting $\Pi_{\alpha\beta}(q)$. For example, keeping only graphs (a_1) and (a_2) is not correct even perturbatively because the ghost loop is crucial for the transversality of $\Pi_{\alpha\beta}$ already at one loop; adding (a_3) is still not sufficient for an SDE analysis because (beyond one loop) $q^\alpha[(a_1) + (a_2) + (a_3)]_{\alpha\beta} \neq 0$.

As we will see in what follows, the application of the pinch technique to the conventional SDEs of the NAGTs gives rise to new equations endowed with special properties. The building blocks of the new SDEs are modified Green's functions obeying Abelian all-order Ward identities instead of the Slavnov–Taylor identities satisfied by their conventional counterparts. As a result, and contrary to the standard case explained earlier, the new equation for the gluon self-energy can be truncated gauge invariantly at any order in the dressed-loop expansion.

6.3 The pinch technique algorithm for Schwinger–Dyson equations

At the end of Chapter 4, we saw, in a one-loop context, how the PT algorithm can be translated in Batalin–Vilkovisky language. More generally, the one-loop procedure described there carries over practically unaltered to the corresponding SDEs. This is so because of the following observations:

1. The pinching momenta will be always determined from the tree-level decomposition of Eqs. (1.41), (1.42), and (1.43).
2. Their action is completely fixed by the structure of the Slavnov–Taylor identities they trigger (Eq. (4.27) for the vertex at hand).

3. The kernels appearing in these Slavnov–Taylor identities are the same as those appearing in the corresponding background-quantum identities, making it always possible to write the result of the action of pinching momenta in terms of auxiliary Green's functions appearing in the latter identities.

The only operational difference is that, in the case of the Schwinger–Dyson equations for the three-gluon vertex (and the quark-gluon vertex, in the case in which quarks are included), all three external legs will be off shell. This is, of course, unavoidable, given that these (fully dressed) vertices are nested in the SDE of the off-shell gluon self-energy (see, e.g., diagram (a_1) of Figure 6.4), and their legs inside the diagrams are irrigated by the virtual off-shell momenta. As a result, the equations of motion usually employed to kill some of the resulting pinching terms should not be used in this case; therefore, the corresponding terms, proportional to inverse self-energies, do not drop out but rather, form part of the resulting background-quantum identity.

The PT rules for the construction of SDEs may be summarized as follows [24]:

1. For the SDEs of vertices, with all three external legs off shell, the pinching momenta, coming from the (only) external three-gluon vertex undergoing the decomposition (1.41), generate at most four types of terms: one is a genuine vertexlike contribution that must be included in the final PT answer for the vertex under construction; the remaining three terms will form part of the emerging background-quantum identities (and thus would be discarded from the PT vertex). These latter terms have a very characteristic structure that facilitates their identification in the calculation. Specifically, one of them is always proportional to the auxiliary function $\Gamma_{\Omega A^*}$, whereas the other two are proportional to the inverse propagators of the fields entering into the two legs that did not undergo the PT decomposition.

2. In the case of the new SDE for the gluon propagator, the pinching momenta will only generate pieces proportional to $\Gamma_{\Omega A^*}$, which should be discarded from the PT answer for the gluon two-point function (because they are exactly what cancels against the contribution coming from the corresponding vertices).

6.4 Pinch technique Green's functions from Schwinger–Dyson equations

We are now ready to describe in detail the application of the PT program to the (nonperturbative) case of SDEs. We will concentrate on the SDE of the gluon self-energy,[2] which requires carrying out the PT decomposition of Eq. (1.41)

---

[2] The construction of the (fully off-shell) quark-gluon and three-gluon vertices can be found in [24].

on both sides of the self-energy diagram because both external gluons must be converted into background gluons. This will be achieved through the following three steps [24, 25].

6.4.1 First step: $\Gamma_{AA} \to \Gamma_{\widehat{A}A}$

The first step of the construction is the standard PT step: starting from diagram (a_1) of Figure 6.4, we decompose the tree-level three-gluon vertex according to the usual PT splitting of Eq. (1.41) and concentrate on the Γ^{P} part. We then get

$$(a_1)^{\mathrm{P}} = \mathrm{i}g f^{amn} \int_{k_1} \frac{1}{k_1^2} \Delta_\alpha^\nu(k_2) k_1^\mu \Gamma_{A_\mu^m A_\nu^n A_\beta^b}(k_2, -q). \tag{6.5}$$

At this point, the application of the Slavnov–Taylor identity (4.24) together with Eq. (4.25) and the Faddeev–Popov equation (4.26) results in the following terms:

$$(a_1)^{\mathrm{P}} = \mathrm{i}g f^{amn} \int_{k_1} D(k_1) \Delta_\alpha^\nu(k_2) \Gamma_{c^m A_\nu^n A_b^{*\gamma}}(k_2, -q) \Gamma_{A_\gamma A_\beta}(q)$$

$$+ g f^{amn} \int_{k_1} D(k_1) \left[\Gamma_{c^m A_\beta^b A_\alpha^{*n}}(-q, k_2) - \mathrm{i}\frac{k_{2\alpha}}{k_2^2} \Gamma_{c^m A_\beta^b \bar{c}^n}(-q, k_2) \right]$$

$$= (r_1)^{\mathrm{P}} + (r_2)^{\mathrm{P}}. \tag{6.6}$$

Clearly, using the SDE of the auxiliary function $\Gamma_{\Omega A^*}$, shown in Eq. (4.44), one has immediately that

$$(r_1)^{\mathrm{P}} = -\mathrm{i}\Gamma_{\Omega_\alpha^a A_d^{*\gamma}}(q) \Gamma_{A_\gamma^d A_\beta^b}(q). \tag{6.7}$$

This would be half of the pinching contribution coming from the vertex in the S-matrix pinch technique.

As far as the term $(r_2)^{\mathrm{P}}$ is concerned, its general structure suggests that the first term in the square brackets should give rise to the ghost quadrilinear vertex, whereas the second term in that same bracket, when added to diagram (a_3), should symmetrize the trilinear ghost-gluon coupling. It turns out that this expectation is essentially correct, but its realization is not immediate because we see, for example, that $(r_2)^{\mathrm{P}}$ contains a tree-level $[(k_2^2)^{-1}]$ instead of a full $[D(k_2)]$ ghost propagator and that it is unclear how one would generate, e.g., diagrams (b_7) or (b_9) of Figure 6.6. The solution to this apparent mismatch is rather subtle: one must employ the SDE satisfied by the ghost propagator, as shown in Figure 6.5. This SDE is common to both the R_ξ-gauge and the BFM, given that there are no background ghosts, and reads

$$\mathrm{i}D^{dn'}(k_2) = \mathrm{i}\frac{\delta^{dn'}}{k_2^2} + \mathrm{i}\frac{\delta^{dg}}{k_2^2} \left[-\Gamma'_{c^g \bar{c}^{g'}}(k_2) \right] \mathrm{i}D^{g'n'}(k_2), \tag{6.8}$$
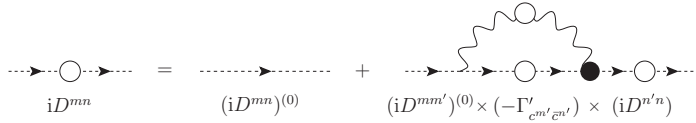
Figure 6.5. The Schwinger–Dyson equation (6.8) satisfied by the ghost propagator.

with $\Gamma'_{c\bar{c}}$ being given by $\Gamma_{c\bar{c}}$ minus its tree-level part; notice that multiplying the preceding equation by k_2^2, using the Faddeev–Popov equation (4.21), and dropping the color factor $\delta^{dn'}$, we can rewrite the ghost SDE as

$$k_{2\alpha} D(k_2) = \frac{k_{2\alpha}}{k_2^2} - \Gamma'_{cA_\alpha^*}(k_2)D(k_2). \tag{6.9}$$

Taking advantage of this last equation, we can rewrite $(r_2)^{\mathrm{P}}$ as the sum of the following two terms:

$$(s_1)^{\mathrm{P}} = -\mathrm{i}g f^{amn} \int_{k_1} k_{2\alpha} D(k_1)D(k_2)\Gamma_{c^m A_\beta^b \bar{c}^n}(-q, k_2) \tag{6.10}$$

$$(s_2)^{\mathrm{P}} = -g f^{amn} \int_{k_1} \mathrm{i}D(k_1) \Big[\mathrm{i}\Gamma_{c^m A_\beta^b A_\alpha^{*n}}(-q, k_2)$$

$$+ \Gamma'_{cA_\alpha^*}(k_2)D(k_2)\Gamma_{c^m A_\beta^b \bar{c}^n}(-q, k_2) \Big]. \tag{6.11}$$

The term $(s_1)^{\mathrm{P}}$ symmetrizes the trilinear ghost-gluon coupling, and one has

$$(s_1)^{\mathrm{P}} + (a_3) = (b_3) \tag{6.12}$$

(with (b_3) shown in Figure 6.6). The term $(s_2)^{\mathrm{P}}$ will instead be responsible for generating all the missing diagrams needed to convert Γ_{AA} into $\Gamma_{\hat{A}A}$. To see how this happens, we denote by $(s_{2a})^{\mathrm{P}}$ and $(s_{2b})^{\mathrm{P}}$ the two terms appearing in the square brackets of $(s_2)^{\mathrm{P}}$ and concentrate on the first one. Making use of the SDE (4.43) satisfied by the auxiliary function Γ_{cAA^*}, we get

$$(s_{2a})^{\mathrm{P}} = g^2 C_A \delta^{ab} g_{\alpha\beta} \int_{k_1} D(k_1)$$

$$+ g^2 f^{amd} f^{dnr} \int_{k_1} \int_{k_3} D(k_1)\Delta_\alpha^\rho(k_3)D(k_4)\mathcal{K}_{c^m A_\beta^b A_\rho^r \bar{c}^n}(-q, k_3, k_4)$$
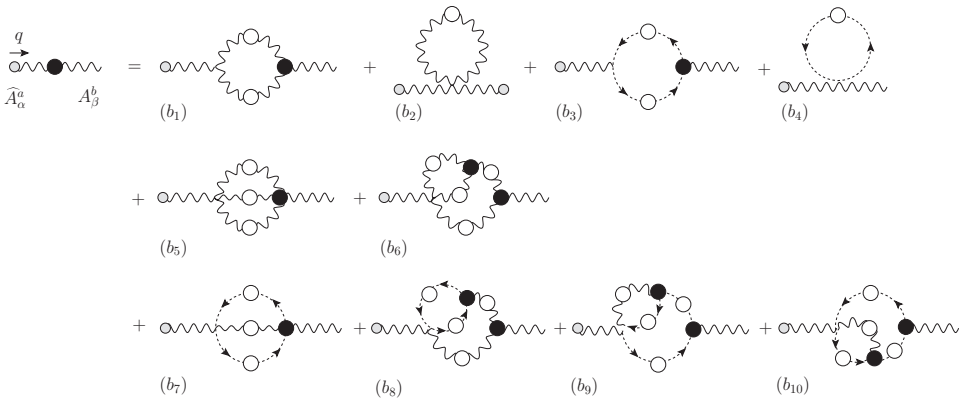
$$= (b_4) + (b_7) + (b_8) + (b_{10}). \tag{6.13}$$

Figure 6.6. Schwinger–Dyson equation satisfied by the gluon self-energy $-\Gamma_{\widehat{A}A}$. The symmetry factors of the diagrams are $s(b_1, b_2, b_6) = 1/2$ and $s(b_5) = 1/6$, and all the remaining diagrams have $s = -1$.

Using the SDE (4.42) satisfied by Γ_{cA^*}, we then obtain

$$(s_{2b})^{\mathrm{P}} = \mathrm{i}g^2 f^{amd} f^{drs} \int_{k_1} \int_{k_3} D(k_1) \Gamma_{c^n A_\rho^r \bar{c}^s}(k_3, k_4) \Delta_\alpha^\rho(k_3) D(k_4) D(k_2)$$
$$\times \Gamma_{c^m A_\beta^b \bar{c}^n}(-q, k_2)$$
$$= (b_9). \tag{6.14}$$

In addition, because diagrams (a_2), (a_4), (a_5), and (a_6) carry over to the corresponding BFM diagrams (b_2), (b_5), (b_6), and (b_{11}), and $(a_1)^{\mathrm{F}} = (b_1)$, we finally find the identity

$$(r_2)^{\mathrm{P}} + \left[(a_1)^{\mathrm{F}} + \sum_{i=2}^{6} (a_i) \right] = \sum_{i=1}^{11} (b_i), \tag{6.15}$$

and therefore

$$-\Gamma_{A_\alpha^a A_\beta^b}(q) = -\mathrm{i}\Gamma_{\Omega_\alpha^a A_d^{*\gamma}}(q) \Gamma_{A_\gamma^d A_\beta^b}(q) - \Gamma_{\widehat{A}_\alpha^a A_\beta^b}(q), \tag{6.16}$$

which coincides with the background-quantum identity (4.31).

6.4.2 Second step: $\Gamma_{\widehat{A}A} \to \Gamma_{A\widehat{A}}$

The second step in the propagator construction is to employ the obvious relation

$$\Gamma_{\widehat{A}_\alpha^a A_\beta^b}(q) = \Gamma_{A_\alpha^a \widehat{A}_\beta^b}(q), \tag{6.17}$$

that is, to interchange the background and quantum legs (the SDE for the self-energy $-\Gamma_{A\widehat{A}}$ is shown in Figure 6.7). This apparently trivial operation introduces
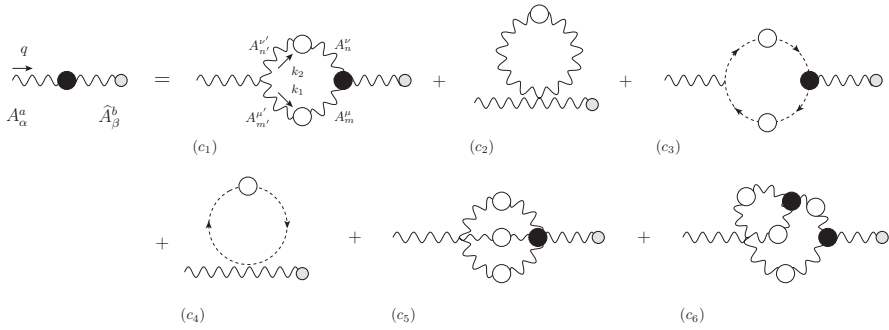
Figure 6.7. Schwinger–Dyson equation satisfied by the gluon self-energy $-\Gamma_{A\widehat{A}}$. The symmetry factors of the diagrams are $s(c_1, c_2, c_6) = 1/2$, $s(c_3, c_4, c_7) = -1$, $s(c_5) = 1/6$.
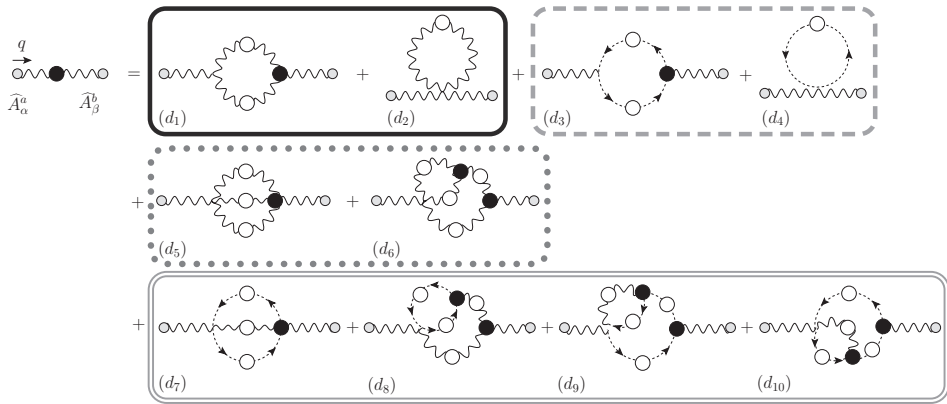

Figure 6.8. Schwinger–Dyson equation satisfied by the gluon self-energy $-\Gamma_{\widehat{A}\widehat{A}}$. The symmetry factors are the same as the one described in Figure 6.5. The different boxes show gauge-invariant subgroups: one-loop dressed gluon (solid line) and ghost (dashed line) contributions and two-loop dressed gluon (dotted line) and ghost (double line) contributions (see the discussion in Section 6.4.4).

a considerable simplification. First, it allows for the identification of the pinching momenta from the usual PT decomposition of the (tree level) Γ appearing in diagram (c_1) of Figure 6.7 (something not directly possible from diagram (b_1)); thus, from the operational point of view, we remain on familiar ground. In addition, it avoids the need to employ the (formidably complicated) BQI for the four-gluon vertex; indeed, the equality between diagrams (c_5), (c_6), and (c_7) of Figure 6.7 and diagrams (d_5), (d_6), and (d_{11}) of Figure 6.8 is now immediate (as it was before, between diagrams (a_4), (a_5), and (a_6) and (b_5), (b_6), and (b_{11}) of Figures 6.6 and 6.7, respectively).

6.4.3 Third step: $\Gamma_{A\widehat{A}} \to \Gamma_{\widehat{A}\widehat{A}}$

We now turn to diagram (c_1) and concentrate on its pinching part given by

$$(c_1)^{\mathrm{P}} = \mathrm{i}gf^{amn} \int_{k_1} \frac{1}{k_1^2} \Delta_\alpha^\nu(k_2) k_1^\mu \Gamma_{A_\mu^m A_\nu^n \widehat{A}_\beta^b}(k_2, -q).$$ (6.18)

Notice the appearance of the full BFM vertex $\Gamma_{AA\widehat{A}}$ instead of the standard Γ_{AAA} (in the R_ξ). The Slavnov–Taylor identity satisfied by this vertex can be derived by means of the methods introduced in the previous chapter; the result is[3]

$$k_1^\mu \Gamma_{\widehat{A}_\alpha^a A_\mu^m A_\nu^n}(k_1, k_2) = [k_1^2 D^{mm'}(k_1)] \left\{ \Gamma_{c^{m'} A_\nu^n A_e^{*\epsilon}}(k_2, q) \Gamma_{\widehat{A}_\alpha^a A_\epsilon}(q) \right.$$

$$\left. + \Gamma_{c^{m'} \widehat{A}_\alpha^a A_e^{*\epsilon}}(q, k_2) \Gamma_{A_\epsilon^e A_\nu^n}(k_2) \right\}$$

$$- \mathrm{i}gf^{amn}(k_1^2 g_{\alpha\nu} - k_{1\alpha} k_{2\nu}),$$ (6.19)

where the tree-level term accounts for working with the reduced Slavnov–Taylor functional. This identity can be further manipulated by using Eq. (4.25) and the Faddeev–Popov equation satisfied by $\Gamma_{c\widehat{A}A^*}$ to get

$$k_1^\mu \Gamma_{\widehat{A}_\alpha^a A_\mu^m A_\nu^s}(k_1, k_2) = [k_1^2 D^{mm'}(k_1)] \left\{ \Gamma_{c^{m'} A_\nu^n A_e^{*\epsilon}}(k_2, q) \Gamma_{\widehat{A}_\alpha^a A_\epsilon}(q) \right.$$

$$\left. + \Gamma_{c^{m'} \widehat{A}_\alpha^a A_e^{*\epsilon}}(q, k_2)(\Delta^{-1})_{\epsilon\nu}^{en}(k_2) + k_{2\nu} \Gamma_{c^{m'} \widehat{A}_\alpha^a \bar{c}^n}(q, k_2) \right\}$$

$$- \mathrm{i}gf^{amn} k_1^2 g_{\alpha\nu}.$$ (6.20)

Consider first the terms that appear in braces. When inserted back into Eq. (6.18) (we indicate the resulting expression as $(r_1)^{\mathrm{P}}$), we see that one gets precisely the same contributions found in Eq. (6.6), the only difference being that the A_β^b gluon field appearing there is now the background field $\widehat{A}_\beta^b$. Therefore, following step by step the same procedure used in that case, we find that (see Figure 6.8 for the diagrams corresponding to each (d_i))

$$(r_1)^{\mathrm{P}} + (c_3) = -\mathrm{i}\Gamma_{\Omega_\alpha^a A_\epsilon^{*\epsilon}}(q) \Gamma_{A_\epsilon^e \widehat{A}_\beta^b}(q)$$

$$+ (d_3) + (d_4) + (d_7) + (d_8) + (d_9) + (d_{10}).$$ (6.21)

Finally, adding diagram (c_2) to the remaining tree-level term of Eq. (6.20), one gets

$$(r_2)^{\mathrm{P}} + (c_2) = g^2 C_A \delta^{ab} \int_{k_1} \Delta_{\alpha\beta}(k_1) + (c_2) = (d_2).$$ (6.22)

---

[3] Given a Green's function involving background as well as quantum fields, it is clear that if we contract it with the momentum corresponding to a background leg, we will obtain a linear Ward identity (see, e.g., Eqs. (6.28)–(6.31)), whereas if we contract it with the momentum corresponding to a quantum leg, we will obtain a nonlinear Slavnov–Taylor identity.

Putting everything together, and using the standard PT identity $(c_1)^F = (d_1)$, we get

$$(r_1)^P + (r_2)^P + \left[(c_1)^F + \sum_{i=2}^{7}(c_i) \right] = -i\Gamma_{\Omega_\alpha^a A_\epsilon^{*e}}(q)\Gamma_{A_\epsilon^e \widehat{A}_\beta^b}(q) + \sum_{i=1}^{11}(d_i), \quad (6.23)$$

and therefore

$$- \Gamma_{A_\alpha^a \widehat{A}_\beta^b}(q) = -i\Gamma_{\Omega_\alpha^a A_\epsilon^{*e}}(q)\Gamma_{A_\epsilon^e \widehat{A}_\beta^b}(q) - \Gamma_{\widehat{A}_\alpha^a \widehat{A}_\beta^b}(q), \quad (6.24)$$

which is the background-quantum identity (4.32).

6.4.4 The final rearrangement and the new Schwinger–Dyson equation

Pulling together all the intermediate results, we see that the PT procedure has given rise to a new Schwinger–Dyson series:

$$i\Gamma_{A_\alpha A_\beta} + 2\Gamma_{\Omega_\alpha A^{*\gamma}}\Gamma_{A_\gamma A_\beta} - i\Gamma_{\Omega_\alpha A^{*\gamma}}\Gamma_{A_\gamma A_\epsilon}\Gamma_{\Omega_\beta A^{*\epsilon}} = i\sum_{1=1}^{11}(d_i)_{\alpha\beta}. \quad (6.25)$$

By Lorentz-decomposing the auxiliary function $\Gamma_{\Omega A^*}(q)$ according to Eq. (4.34) and trading the gluon two-point function for the gluon propagator, we arrive at the equation (viz. Eq. (4.35))

$$\Delta^{-1}(q^2)[1 + G(q^2)]^2 P_{\alpha\beta}(q) = q^2 P_{\alpha\beta}(q) + i\sum_{1=1}^{11}(d_i)_{\alpha\beta}. \quad (6.26)$$

Equivalently, the new SDE (6.26) can be cast into a more conventional form by isolating on the left-hand side (lhs) the inverse of the unknown quantity, thus writing

$$\Delta^{-1}(q^2)P_{\alpha\beta}(q) = \frac{q^2 P_{\alpha\beta}(q) + i\sum_{1=1}^{11}(d_i)_{\alpha\beta}}{[1 + G(q^2)]^2}. \quad (6.27)$$

As a consequence of the all-order Ward identities satisfied by the full vertices appearing in the diagrams defining the PT-background Feynman gauge self-energy (Figure 6.8), the new SDE (6.27) has a special transversality property: in fact, gluonic and ghost contributions are separately transverse, and, in addition, no mixing between the one- and two-loop dressed diagrams will take place.

To prove this, one needs to know the Ward identity corresponding to the four fully dressed vertices appearing in $\widehat{\Pi}$: $\Gamma_{\widehat{A}AA}$, $\Gamma_{c\widehat{A}\bar{c}}$, $\Gamma_{\widehat{A}AAA}$, and, finally, $\Gamma_{c\widehat{A}\bar{c}A}$. One way to derive them is to differentiate the Ward identity functional (4.14) with

respect to the corresponding field combination in which the background field has been replaced by the corresponding gauge parameter ϑ. On the other hand, one can also write the corresponding tree-level Ward identities and then use linearity to generalize them to all orders. In either case, the following results are obtained:

$$q^{\alpha}\Gamma_{\widehat{A}_{\alpha}^{a}A_{\mu}^{m}A_{\nu}^{n}}(k_1, k_2) = gf^{amn}\left[\Delta_{\mu\nu}^{-1}(k_1) - \Delta_{\mu\nu}^{-1}(k_2)\right] \tag{6.28}$$

$$q^{\alpha}\Gamma_{c^n\widehat{A}_{\alpha}^{a}\bar{c}^m}(q, -k_1) = igf^{amn}\left[D^{-1}(k_2) - D^{-1}(k_1)\right] \tag{6.29}$$

$$q^{\alpha}\Gamma_{\widehat{A}_{\alpha}^{a}A_{\beta}^{b}A_{\mu}^{m}A_{\nu}^{n}}(k_1, k_2, k_3) = gf^{adb}\Gamma_{A_{\beta}^{d}A_{\mu}^{m}A_{\nu}^{n}}(k_2, k_3)$$
$$+ gf^{adm}\Gamma_{A_{\mu}^{d}A_{\beta}^{b}A_{\nu}^{n}}(k_1, k_3)$$
$$+ gf^{adn}\Gamma_{A_{\nu}^{d}A_{\beta}^{b}A_{\mu}^{m}}(k_1, k_2) \tag{6.30}$$

$$q^{\alpha}\Gamma_{c^n\widehat{A}_{\alpha}^{a}A_{\beta}^{b}\bar{c}^m}(q, k_3, -k_1) = gf^{adb}\Gamma_{c^n A_{\beta}^{d}\bar{c}^m}(q + k_3, -k_1)$$
$$+ gf^{adm}\Gamma_{c^n A_{\beta}^{b}\bar{c}^d}(k_3, q - k_1)$$
$$+ gf^{adn}\Gamma_{c^d A_{\beta}^{b}\bar{c}^m}(k_3, -k_1). \tag{6.31}$$

We shall consider then the one-loop dressed gluonic contributions given by the combination $(d_1) + (d_2)$ of Figure 6.8. Using the Ward identity (6.28), we get

$$q^{\beta}(d_1)_{\alpha\beta}^{ab} = -g^2 C_A \delta^{ab} q_{\alpha} \int_k \Delta_{\mu}^{\mu}(k), \tag{6.32}$$

whereas by simply computing the divergence of the tree-level vertex $\Gamma_{\widehat{A}\widehat{A}AA}$, we get

$$q^{\beta}(d_2)_{\alpha\beta}^{ab} = g^2 C_A \delta^{ab} q_{\alpha} \int_k \Delta_{\mu}^{\mu}(k). \tag{6.33}$$

Thus, clearly,

$$q^{\beta}\left[(d_1) + (d_2)\right]_{\alpha\beta}^{ab} = 0. \tag{6.34}$$

Exactly the same procedure shows that for the one-loop-dressed ghost contribution,

$$q^{\beta}(d_3)_{\alpha\beta}^{ab} = -2g^2 C_A \delta^{ab} q_{\alpha} \int_k D(k) = -q^{\beta}(d_4)_{\alpha\beta}^{ab}, \tag{6.35}$$

and therefore that

$$q^{\beta}\left[(d_3) + (d_4)\right]_{\alpha\beta}^{ab} = 0. \tag{6.36}$$

For the two-loop dressed contributions, the proof is to a certain extent more involved. Begin with the gluonic contributions. Using the Ward identity (6.30), we see that diagram (d_5) would give rise, in principle, to three different terms.

However, it is straightforward to prove that these terms are all equal modulo rela-beling of momenta and Lorentz or color indices. Thus, recalling that this diagram carries a symmetry factor of $1/6$, we get

$$q^\beta (d_5)^{ab}_{\alpha\beta} = \frac{\mathrm{i}}{2} g f^{bmn} \Gamma^{(0)}_{\widehat{A}^a_\alpha A^m_{\mu'} A^g_{\gamma'} A^e_{\epsilon'}} \int_k \int_\ell \Delta^{\epsilon'\epsilon}(k) \Delta^{\gamma'\gamma}(\ell+k) \Gamma_{A^g_\gamma A^e_\epsilon A^n_\mu}(k,\ell)$$
$$\times \Delta^{\mu'\mu}(\ell+q), \tag{6.37}$$

while the remaining graph gives (after making use of the full Bose symmetry of the three-gluon vertex)

$$q^\beta (d_6)^{ab}_{\alpha\beta} = \frac{\mathrm{i}}{2} g f^{bmn} \Gamma^{(0)}_{\widehat{A}^a_\alpha A^m_{\mu'} A^g_{\gamma'} A^e_{\epsilon'}} \int_k \int_\ell \Delta^{\epsilon'\epsilon}(k) \Delta^{\gamma'\gamma}(\ell+k) \Gamma_{A^g_\gamma A^e_\epsilon A^{n'}_{\nu'}}(k,\ell)$$
$$\times \left[\Delta^{\nu'\nu}(\ell) g^{\mu'}_\nu - \Delta^{\mu'\mu}(\ell+q) g^{\nu'}_\mu \right]. \tag{6.38}$$

Now, on the one hand, the first term in the square brackets must integrate to zero because the integral is independent of q, and therefore the free Lorentz index α cannot be saturated. On the other hand, the second term is exactly equal but opposite in sign to the one appearing in Eq. (6.37) so that we obtain

$$q^\beta \left[(d_5) + (d_6) \right]^{ab}_{\alpha\beta} = 0. \tag{6.39}$$

Finally, we turn to the two-loop dressed ghost contributions. Using the Ward identity (6.31), we see that the divergence of diagram (d_7) gives us three terms, namely,

$$q^\beta (d_7)^{ab}_{\alpha\beta} = -\mathrm{i} \Gamma^{(0)}_{c^{m'} \widehat{A}^a_\alpha A^{r'}_{\rho'} \bar{c}^{n'}} \int_k \int_\ell D^{m'm}(\ell+k) D^{n'n}(\ell+q) \Delta^{\rho'\rho}_{r'r}(k)$$
$$\times \left[g f^{ber} \Gamma_{c^n A^e_\rho \bar{c}^e}(k-q, -\ell-k) + g f^{ben} \Gamma_{c^e A^r_\rho \bar{c}^m}(k, -\ell-k) \right.$$
$$\left. + g f^{ben} \Gamma_{c^n A^r_\rho \bar{c}^n}(k, -q-\ell-k) \right]. \tag{6.40}$$

Each one of these three terms can be easily shown to cancel exactly against the individual divergences of the remaining three graphs. To see this in detail, let us consider, for example, diagram (d_{10}) and use the Ward identity (6.29) to obtain

$$q^\beta (d_{10})^{ab}_{\alpha\beta} = -\mathrm{i} g f^{bmn} \Gamma^{(0)}_{c^m \widehat{A}^a_\alpha A^r_\rho \bar{c}^d} \int_k \int_\ell \Delta^{\rho'\rho}(k) \Gamma_{c^d A^r_\rho \bar{c}^n}(k, -q-\ell-k)$$
$$\times D(\ell+q) \left[D(\ell+k) - D(\ell+k+q) \right]. \tag{6.41}$$

We see that the second term in the square brackets will integrate to zero, whereas the first term will cancel exactly the third term appearing in the square brackets of Eq. (6.40). It is not difficult to realize that the same pattern will be encountered

when calculating the divergence of diagrams (d_8) and (d_9) so that one has the identity

$$q^\beta \left[(d_7) + (d_8) + (d_9) + (d_{10}) \right]^{ab}_{\alpha\beta} = 0, \tag{6.42}$$

which then concludes our proof of the special transversality properties of the new Schwinger–Dyson series.

This special property has far-reaching practical consequences for the treatment of the Schwinger–Dyson series [24, 25]. Specifically, it furnishes a systematic truncation scheme that preserves the transversality of the answer. For example, keeping only the diagrams in the first group, we obtain the truncated SDE

$$\Delta^{-1}(q^2) P_{\alpha\beta}(q) = \frac{q^2 P_{\alpha\beta}(q) + i[(d_1) + (d_2)]_{\alpha\beta}}{[1 + G(q^2)]^2}, \tag{6.43}$$

and from Eq. (6.34), we know that $[(d_1) + (d_2)]_{\alpha\beta}$ is transverse, i.e.,

$$[(d_1) + (d_2)]_{\alpha\beta} = (d - 1)^{-1}[(d_1) + (d_2)]^\mu_\mu P_{\alpha\beta}(q). \tag{6.44}$$

Thus, the transverse projector $P_{\alpha\beta}(q)$ appears *exactly* on both sides of Eq. (6.43); one may susbsequently isolate the scalar cofactors on both sides, obtaining a scalar equation of the form

$$\Delta^{-1}(q^2) = \frac{q^2 + i[(d_1) + (d_2)]^\mu_\mu}{[1 + G(q^2)]^2}. \tag{6.45}$$

A truncated equation similar to Eq. (6.43) may be written for any other of the four groups previously isolated, or for sums of these groups, without compromising the transversality of the answer. The price one has to pay for this advantageous situation is rather modest and consists in considering the additional equation determining the scalar function $G(q^2)$; notice, however, that one can approximate this function via a dressed-loop expansion without jeopardizing the transversality of $\Pi_{\alpha\beta}(q)$, given that $[1 + G(q^2)]^2$ affects only the size of the scalar prefactor.

Let us conclude by noticing that in going from Eq. (6.26) to Eq. (6.27), one essentially chooses to retain the original propagator $\Delta(q)$ as the unknown quantity to be dynamically determined from the Schwinger–Dyson equation. There is, of course, an alternative strategy: one may define a new *variable* from the quantity appearing on the lhs of Eq. (6.26), namely,

$$\widehat{\Delta}(q) \equiv \left[1 + G(q^2) \right]^{-2} \Delta(q), \tag{6.46}$$

which leads to a new form for Eq. (6.26):

$$\widehat{\Delta}^{-1}(q^2)P_{\alpha\beta}(q) = q^2 P_{\alpha\beta}(q) + \mathrm{i}\sum_{i=1}^{11}(d_i)_{\alpha\beta}. \qquad (6.47)$$

Obviously, the special transversality properties established earlier hold as well for Eq. (6.47); for example, one may truncate it gauge invariantly as

$$\widehat{\Delta}^{-1}(q^2)P_{\alpha\beta}(q) = q^2 P_{\alpha\beta}(q) + \mathrm{i}[(d_1) + (d_2)]_{\alpha\beta}. \qquad (6.48)$$

Should one opt for treating $\widehat{\Delta}(q)$ as the new unknown quantity, then an additional step must be carried out: one must use Eq. (6.46) to rewrite the entire rhs of Eq. (6.47) in terms of $\widehat{\Delta}$ instead of Δ, i.e., carry out the replacement $\Delta \to [1 + G]^2 \, \widehat{\Delta}$ *inside* every diagram on the rhs of Eq. (6.47) that contains Δs.

Therefore, whereas Eq. (6.43) furnishes a gauge-invariant approximation for the conventional gluon self-energy $\Delta(q)$, Eq. (6.47) is the gauge-invariant approximation for the effective PT self-energy $\widehat{\Delta}(q)$. The crucial point is that one may switch from one to the other by means of Eq. (6.46). For practical purposes, this means, for example, that one may get a gauge-invariant approximation not just for the PT quantity (background Feynman gauge) but also for the conventional self-energy computed in the Feynman gauge. Equation (6.46) plays an instrumental role in this entire construction, allowing one to convert the Schwinger–Dyson series into a dynamical equation for either $\widehat{\Delta}(q)$ or $\Delta(q)$.

6.4.5 Truncation of the pinch technique Schwinger–Dyson equation

The new Schwinger–Dyson series projected by the pinch technique has both theoretical and practical advantages. On the one hand, the main theoretical advantage is that the various fully dressed graphs organize themselves into gauge-invariant subsets, thus allowing for a systematic gauge-invariant truncation. On the other hand, at the practical level, this property reduces the number of coupled SDEs that one has to consider to maintain the gauge (BRST) symmetry of the theory to only two: the one for the gluon self-energy, given by, e.g., the first gauge-invariant subset only (i.e., $[(d_1) + (d_2)]_{\alpha\beta}$ in Figure 6.8), and the Schwinger–Dyson equation satisfied by the full three-gluon vertex. This is to be contrasted to what happens within the conventional formulation where the equations for all vertices must be considered, or else the transversality of the gluon propagator is violated (which is what usually happens).

However, even the PT analysis does not furnish a simple diagrammatic truncation, analogous to that of the gluon self-energy, for the Schwinger–Dyson equation satisfied by the three-gluon vertex $\Gamma_{\widehat{A}_\alpha A_\mu A_\nu}(k_1, k_2)$. Thus, if one were to truncate the equation for the three-gluon vertex by discarding some of the graphs appearing

in it, the validity of the all-order Ward identity (6.28) would be violated; this, in turn, would lead immediately to the violation of the transversality property of the subset kept, thus making the entire truncation scheme collapse.

One should adopt the following strategy instead: given that the proposed truncation scheme hinges crucially on the validity of Eq. (6.28), one should start with an approximation that manifestly preserves it. The way to enforce this, therefore, is through the gauge technique, as described in Chapter 5.

6.5 Solutions of the pinch technique Schwinger–Dyson equations and comparison with lattice data

We will next focus on a particular application of the powerful machinery offered by the truncation scheme introduced in the previous section. In particular, we will study gauge invariantly the coupled SDEs of the gluon and ghost propagators and compare the results obtained to recent lattice data. To this end, we will do the following:

1. We will truncate (gauge invariantly) the gluon propagator SDE by keeping only the one-loop dressed contributions; that is, we only consider the first two blocks appearing in Figure 6.8. Recall that when evaluating these diagrams, one must employ the BFM Feynman rules. Note also the following crucial point: the (background) three-gluon vertex $\Gamma_{\widehat{A}AA}$ and the ghost vertex $\Gamma_{c\widehat{A}\bar{c}}$ appearing in the corresponding diagrams must be fully dressed and satisfy the correct Ward identities, namely, Eqs. (6.28) and (6.29), respectively, to enforce the transversality of the resulting gluon self-energy.

2. For the ghost SDE, we use the equation shown in Figure 6.5. Notice that the ghost vertex appearing in the SDE is the conventional one, $\Gamma_{cA\bar{c}}$; therefore, one may employ a different approximation than the one used for the background ghost vertex. In particular, according to lattice studies [26, 27], the vertex $\Gamma_{cA\bar{c}}$ may be accurately approximated simply by its tree-level expression. The ability to employ a different treatment for the two ghost vertices, without compromising gauge invariance, is indicative of the versatility of the new truncation scheme introduced earlier.[4]

3. For the SDE (4.44) governing the dynamics of the auxiliary function $\Gamma_{\Omega A^*}$, the vertex Γ_{AcA^*} will be approximated by its tree-level value.[5]

---

[4] Notice also that, whereas the background ghost vertex satisfies a linear Ward identity, which can be solved through a gauge technique ansatz, the conventional vertex satisfies a Slavnov–Taylor identity of rather limited usefulness.

[5] This vertex has not been studied on the lattice; the only constraints are the ones imposed by the Faddeev–Popov equation (4.26), relating it with the conventional ghost vertex, that are indeed satisfied by our tree-level choice for both vertices.

We then have the following equations:

$$\Delta^{-1}(q^2)P_{\alpha\beta}(q) = \frac{q^2 P_{\alpha\beta}(q) + \mathrm{i}\sum_{1=1}^{4}(d_i)_{\alpha\beta}}{[1 + G(q^2)]^2},$$

$$F^{-1}(q^2) = 1 + g^2 C_{\mathrm{A}} \int_k \left[1 - \frac{(k \cdot q)^2}{k^2 q^2}\right] \Delta(k)D(k + q),$$

$$G(q^2) = \frac{g^2 C_{\mathrm{A}}}{d - 1} \int_k \left[(d - 2) + \frac{(k \cdot q)^2}{k^2 q^2}\right] \Delta(k)D(k + q),$$

$$L(q^2) = \frac{g^2 C_{\mathrm{A}}}{d - 1} \int_k \left[1 - d \frac{(k \cdot q)^2}{k^2 q^2}\right] \Delta(k)D(k + q). \tag{6.49}$$

The concrete dynamics that will give rise to an infrared finite gluon propagator, signaling the dynamical generation of a gluon mass, are inserted into the first of the preceding equations through an appropriate gauge technique ansatz for the fully dressed vertices $\Gamma_{\widehat{A}_\alpha A_\mu A_\nu}(k_1, k_2)$ and $\Gamma_{c\widehat{A}_\alpha \bar{c}}(q, k_1)$, appearing in the diagrams (d_1) and (d_3) of Figure 6.8. Specifically, one expresses $\Gamma_{\widehat{A}_\alpha A_\mu A_\nu}(k_1, k_2)$ and $\Gamma_{c\widehat{A}_\alpha \bar{c}}(q, k_1)$ as a function of the gluon and ghost self-energy, respectively, such that they automatically satisfy the two Ward identities (6.28) and (6.29). In addition, as already explained in the previous chapter, the vertices must contain longitudinally coupled massless (bound state) poles, as is required for triggering the Schwinger mechanism. We will use the following simplified gauge technique ansatze:

$$\Gamma_{\widehat{A}_\alpha A_\mu A_\nu}(k_1, k_2) = \Gamma^{(0)}_{\widehat{A}_\alpha A_\mu A_\nu}(k_1, k_2) + \mathrm{i}\frac{q_\alpha}{q^2}\left[\Pi_{\mu\nu}(k_2) - \Pi_{\mu\nu}(k_1)\right]$$

$$\Gamma_{\widehat{A}_\alpha c\bar{c}}(k_1, k_2) = \Gamma^{(0)}_{\widehat{A}_\alpha c\bar{c}}(k_1, k_2) - \mathrm{i}\frac{q_\alpha}{q^2}\left[L(k_2^2) - L(k_1^2)\right], \tag{6.50}$$

where L denotes the ghost self-energy, $D^{-1}(p^2) = p^2 - \mathrm{i}L(p^2)$. It is elementary to verify that the preceding two vertices indeed satisfy the correct Ward identities (6.28) and (6.29), respectively.

The resulting expression in the Landau gauge[6] for the gluon SDE is too long to be reported here [28]; rather, we show in Figure 6.9 the solution of the full system (6.49) when $G(q^2)$ is approximated by its one-loop expression ($L(q^2)$ is not needed in this case), comparing it with the corresponding lattice data.

Note that, whereas there is good qualitative agreement with the lattice, there is a significant discrepancy (a factor of 2) in the intermediate region of momenta. This,

---

[6] The projection to the Landau gauge is a subtle exercise because one cannot directly set $\xi = 0$ in the integrals given the presence of terms proportional to $1/\xi$ in the background three-gluon vertex. Instead, one has to use the expressions for general ξ, carry out explicitly the set of cancellations produced when the terms proportional to ξ generated by the identity $k^\mu \Delta_{\mu\nu}(k) = -\mathrm{i}\xi k_\nu/k^2$ are used to cancel $1/\xi$ terms, and set $\xi = 0$ only at the very end.
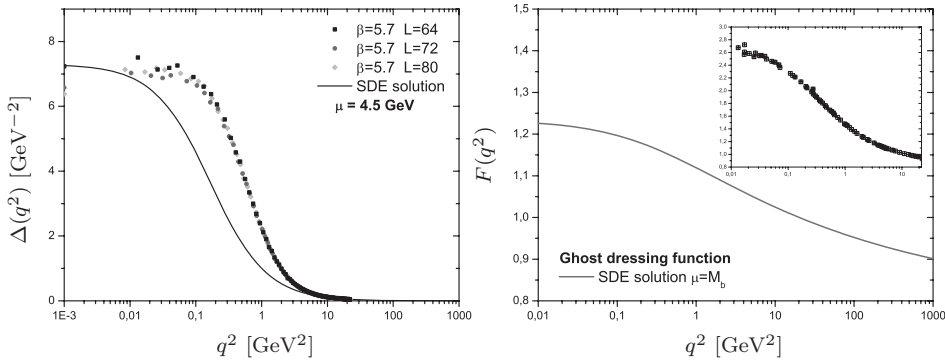
Figure 6.9. (*Left*) The numerical solution for the gluon propagator from the PT modified SDE (solid line) compared to the lattice data of [12]. (*Right*) The ghost-dressing function $p^2 D(p^2)$ obtained from the SDE. In the inset are the lattice data for the same quantity; notice the absence of any enhancement in both cases.

of course, may not come as a surprise, given that (1) the two-loop dressed part of the SDE for the gluon propagator has been omitted (the last two blocks in Figure 6.8) and (2) the auxiliary function $G(q^2)$ has been evaluated at the one-loop level only. Even though this omission has not introduced artifacts (because it was done gauge invariantly), the terms left out are expected to modify precisely the intermediate region, given that both the infrared and ultraviolet limits of the solutions are already captured by the one-loop dressing terms considered.

The finiteness of the ghost-dressing function F in the infrared has an important theoretical consequence related with the so-called Kugo–Ojima confinement criterion, which is already mentioned at the beginning of Chapter 4. In the Kugo–Ojima confinement picture (in covariant gauges), the absence of colored asymptotic states from the physical spectrum of the theory is due to the so-called quartet mechanism [29]. A sufficient condition for the realization of this mechanism (and the meaningful definition of a conserved BRST charge) is that the correlation function $u(q^2)$ defined in Eq. (4.51) satisfies the condition $u(0) = -1$. In addition, as first noted by Kugo [30], in Landau gauge, $u(0)$ is related to the infrared behavior of the ghost-dressing function $F(q^2)$ through the identity $F^{-1}(0) = 1 + u(0)$. This is none other than the second identity of Eq. (4.50), under the additional assumption that $L(0) = 0$. In fact, from the last of Eqs. (6.49), it is straightforward to establish that if both F and Δ are infrared finite, this condition is indeed fulfilled [31, 32]. Therefore, the Kugo–Ojima confinement scenario predicts a divergent ghost-dressing function and vice versa. Interestingly, the same prediction about $F^{-1}(0)$ is obtained when implementing the Gribov–Zwanziger horizon condition [22, 33]: in the infrared region, the ghost propagator diverges more rapidly than at tree level. Evidently, these affirmations are at odds not only with the recent lattice results of the ghost

propagator and the Schwinger–Dyson analysis based on the PT truncation scheme presented here but also with a series of direct lattice simulations of the Kugo–Ojima function itself [34].

6.6 The QCD effective charge

One of the most important successes of the pinch technique is that it allows for the unambiguous extension of the concept of the effective charge [35] from QED to QCD. Such a quantity is of considerable theoretical and phenomenological interest because once correctly defined, it provides a continuous interpolation between two physically distinct QCD regimes: the deep ultraviolet (UV), where perturbation theory works well, and the deep infrared (IR), where nonperturbative techniques must be employed. In fact, the effective charge is intimately connected with two phenomena that are of central importance to QCD: asymptotic freedom in the UV and dynamical gluon mass generation in the IR.

6.6.1 The prototype: The QED effective charge

The quantity that serves as the field-theoretic prototype for guiding our analysis is the effective charge of QED. Consider the bare dressed photon propagator between conserved external currents:

$$\Delta_0^{\mu\nu}(q^2) = \frac{g^{\mu\nu}}{q^2[1 + \mathbf{\Pi}_0(q^2)]}, \tag{6.51}$$

where the dimensionless quantity $\mathbf{\Pi}(q^2)$ is the vacuum polarization, which is independent of the gauge-fixing parameter to all orders. The expression $\Delta_0^{\mu\nu}(q^2)$ is renormalized multiplicatively according to $\Delta_0^{\mu\nu}(q^2) = Z_A \Delta^{\mu\nu}(q^2)$, where Z_A is the wave function renormalization of the photon ($A_0 = Z_A^{1/2} A$). Imposing the on-shell renormalization condition for the photon, we obtain $\mathbf{\Pi}(q^2) = Z_A[1 + \mathbf{\Pi}_0(q^2)]$, where $Z_A = 1 - \mathbf{\Pi}_0(0)$ and $\mathbf{\Pi}(q^2) = \mathbf{\Pi}_0(q^2) - \mathbf{\Pi}_0(0)$; clearly $\mathbf{\Pi}(0) = 0$.

The renormalization procedure introduces, in addition, the standard relations between renormalized and unrenormalized electric charge, $e = Z_e^{-1} e^0 = Z_f Z_A^{1/2} Z_1^{-1} e_0$, where Z_e is the charge renormalization constant, Z_f the wave function renormalization constant of the fermion, and Z_1 the vertex renormalization. From the famous QED relation $Z_1 = Z_f$, a direct consequence of the Ward identity $q^\mu \Gamma_\mu^0(p, p+q) = S_0^{-1}(p+q) - S_0^{-1}(p)$, it follows immediately that $Z_e = Z_A^{-1/2}$.

Given these relations between the renormalization constants, we can now form the following combination:

$$e_0^2 \Delta_0^{\mu\nu}(q^2) = e^2 \Delta^{\mu\nu}(q^2), \tag{6.52}$$

which is invariant under the renormalization group (RG); that is, it maintains the same form before and after renormalization. After pulling out the kinematic factor $(1/q^2)$, one may define the QED effective charge $\alpha_{\text{eff}}(q^2)$, namely,

$$\alpha_{\text{eff}}(q^2) = \frac{\alpha}{[1 + \mathbf{\Pi}(q^2)]}, \tag{6.53}$$

where α is the fine-structure constant.

The QED effective charge of Eq. (6.53) is independent of the gauge-fixing parameter and invariant under the renormalization group to all orders in perturbation theory. Furthermore, given that $\mathbf{\Pi}(0) = 0$, at low energies, the effective charge matches on to the fine-structure constant: $\alpha_{\text{eff}}(0) = \alpha = 1/137.036 \cdots$.

In addition, for asymptotically large values of q^2, i.e., for $q^2 \gg m_f^2$, where m_f denotes the masses of the fermions contributing to the vacuum polarization loop ($f = e, \mu, \tau, \ldots$), $\alpha(q^2)$ matches on to the running coupling $\bar{\alpha}(q^2)$ defined from the RG. At the one-loop level,

$$\alpha_{\text{eff}}(q^2) \overset{q^2 \gg m_f^2}{\longrightarrow} \bar{\alpha}(q^2) = \frac{\alpha}{1 - (\alpha\beta_1/2\pi)\log(q^2/m_f^2)}, \tag{6.54}$$

where $\beta_1 = 2/3 n_f$ is the coefficient of the QED beta function for n_f fermion types.

6.6.2 *The QCD effective charge*

The main difficulty in the generalization of the QED effective charge to QCD (or any other NAGT) is that, unlike the QED vacuum polarization, the conventional QCD gluon self-energy depends explicitly on the gauge-fixing parameter. In addition, with the exception of some special gauges, $Z_1 \neq Z_f$, and therefore the gluon self-energy does not capture, in general, the leading renormalization group logarithms.

The pinch technique solves the preceding difficulties at once: the new gluon self-energy is independent of the gauge-fixing parameter, whereas the Abelian ward identities satisfied by the PT Green's functions (e.g., quark-gluon vertex) restore the crucial equalities $\widehat{Z}_1 = \widehat{Z}_f$ and $Z_g = \widehat{Z}_A^{-1/2}$. In addition, the PT self-energy is process independent [36] (see also Chapter 1) and can be Dyson resummed to all orders [37, 38, 39, 40, 41] (see Chapter 11). Therefore, the construction of the universal and RG-invariant combination analogous to that of Eq. (6.52) is immediate because the quantity

$$\widehat{d}_0(q^2) = g_0^2 \widehat{\Delta}_0(q^2) = g^2(\mu^2)\widehat{\Delta}(q^2, \mu^2) = \widehat{d}(q^2), \tag{6.55}$$

is manifestly RG invariant (viz., μ independent). Then, by virtue of the identity (4.35), we can write equivalently

$$\widehat{d}(q^2) = g^2(\mu^2)\frac{\Delta(q^2, \mu^2)}{\left[1 + G(q^2, \mu^2)\right]^2}. \tag{6.56}$$

It is important to obtain a quantitative confirmation of the μ independence of $\widehat{d}(q^2)$ using as ingredients the individually μ-dependent solutions for $\Delta(q^2, \mu^2)$ and $G(q^2, \mu^2)$ obtained from the system of SDEs given in Eq. (6.49). At this point, one notices a shift in our philosophy, which is, however, dictated only by practical considerations. Specifically, as repeatedly stated, the genuine PT propagator $\widehat{\Delta}(q^2, \mu^2)$ is the one obtained in the Feynman gauge of the BFM, whereas the system of Eq. (6.49) that we consider is formulated in the Landau gauge mainly because the relevant lattice simulations are almost exclusively carried out in this latter gauge. Therefore, we study for the rest of this section the generalized PT effective charge in the BFM Landau gauge (see Section 2.3.4). As is well known, and contrary to what happens in the conventional R_ξ gauges, at one loop in perturbation theory, the coefficient multiplying the renormalization group logarithms does not depend on the specific value of ξ_Q (see Eq. (2.71)). As a result, the asymptotic (ultraviolet) behavior of the two charges (Feynman vs. Landau gauges) will be identical. Note, however, that this is not necessarily so in the infrared; in fact, the freezing value obtained for the Landau gauge effective charge is significantly elevated compared to the value of about 0.5 that one finds for the genuine PT effective charge.

Returning to Eq. (6.56), one may clearly see in Figure 6.10 that all quantities obtained from the aforementioned SDEs, and in particular $\Delta(q^2, \mu^2)$ and $G(q^2, \mu^2)$, display a sizable dependence on the choice of the renormalization point μ. However, when $\Delta(q^2, \mu^2)$ and $G(q^2, \mu^2)$ are used as inputs to form the special combination (6.56), their net μ dependence cancels almost completely against that of $g^2(\mu)$; the latter dependence is obtained from the four-loop beta function corresponding to the minimal-subtraction scheme that we employ for renormalizing the SDEs [42] (see Figure 6.11). Thus one ends up with a nearly μ-independent quantity, as is clearly shown in Figure 6.12.

The next step is to extract out of the dimensionful $\widehat{d}(q^2)$ a dimensionless quantity that would correspond to the QCD effective charge. In the perturbative regime, when momenta are asymptotically large, it is clear that the mass scale is saturated simply by q^2, the bare gluon propagator, and the effective charge is defined by pulling a factor $1/q^2$ out of the corresponding RG-invariant quantity exactly as
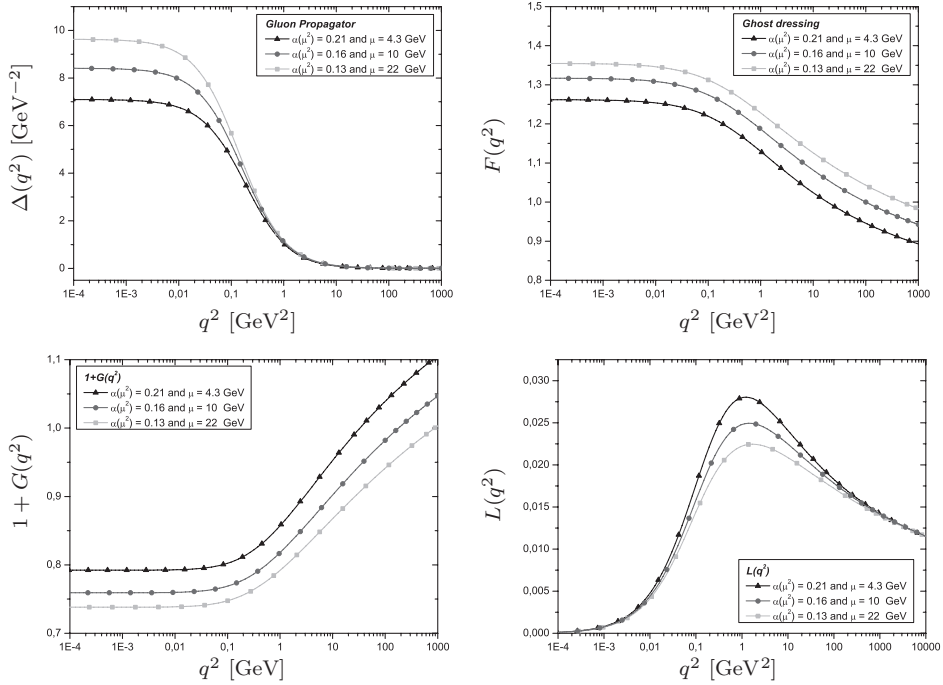
Figure 6.10. The μ dependence of the quantities (*top left*) $\Delta(q^2)$, (*top right*) $F(q^2)$, (*bottom left*) $G(q^2)$, and (*bottom right*) $L(q^2)$ as obtained from solving the system of SDEs (6.49).
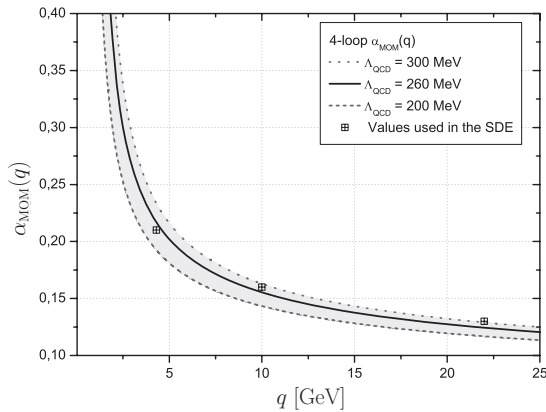

Figure 6.11. The perturbative running coupling in the MOM scheme up to four loops, $\alpha_{\mathrm{MOM}}(q^2)$, for different values of Λ_{QCD}. Black squares represent the values used for $\alpha(\mu^2)$.
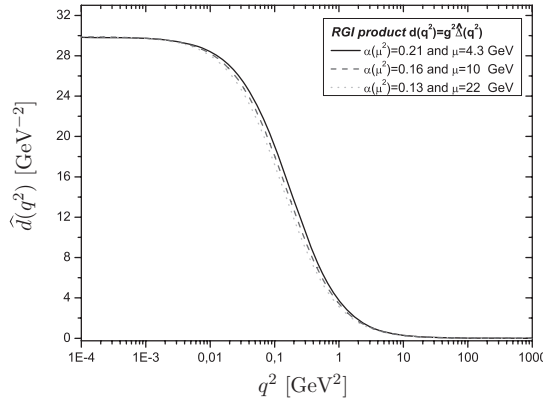
Figure 6.12. The (dimensionful) RG-invariant combination $\widehat{d}(q^2)$ defined in Eq. (6.56).

happens in the QED case. We define

$$\widehat{d}(q^2) = \frac{\overline{g}^2(q^2)}{q^2}, \tag{6.57}$$

with $\overline{g}^2(q^2)$ being the RG-invariant effective charge of QCD; then, at one loop,

$$\overline{g}^2(q^2) = \frac{g^2}{1 + bg^2 \ln\left(q^2/\mu^2\right)} = \frac{1}{b \ln\left(q^2/\Lambda_{\text{QCD}}^2\right)}, \tag{6.58}$$

where Λ_{QCD} denotes an RG-invariant mass scale of a few hundred MeV.

On the other hand, given that the gluon propagator becomes effectively massive in the IR, particular care is needed in deciding exactly what combination of mass scales ought to be pulled out. For example, if one insists on defining the effective charge by trivially factoring out $1/q^2$, the result obtained will be a completely unphysical coupling, vanishing in the deep IR, where QCD is supposed to be strongly coupled. Instead, the correct procedure in such a case is to factor out a massive propagator of the form $[q^2 + m^2(q^2)]^{-1}$, where $m^2(q^2)$ is the dynamical momentum-dependent mass; that is, one must set [23, 31]

$$\widehat{d}(q^2) = \frac{\overline{g}^2(q^2)}{q^2 + m^2(q^2)}. \tag{6.59}$$

Clearly, for $q^2 \gg m^2(q^2)$, the expression on the rhs of Eq. (6.59) goes over to that of Eq. (6.57).

Even though the aforementioned procedure of factoring out a massive propagator was spelled out long ago in the original work on dynamical gluon mass generation [23], owing to a variety of recent developments, this issue deserves some further clarification. To that end, it is instructive to compare the situation with the more familiar, and conceptually more straightforward, case of the electroweak sector of the SM, where the corresponding gauge bosons (W and Z) are also massive, albeit through an entirely different mass-generation mechanism; indeed, despite the difference in their origins, the masses act in a very similar fashion at the level of the RG-invariant quantity associated with the corresponding gauge boson.

In the case of the W-boson, the quantity corresponding to that of Eq. (6.59) would read (Euclidean momenta)

$$\widehat{d}_w(q^2) = \frac{\overline{g}_w^2(q^2)}{q^2 + M_w^2},\tag{6.60}$$

with

$$\overline{g}_w^2(q^2) = g_w^2(\mu)\left[1 + b_w g_w^2(\mu)\int_0^1 dx\,\ln\left(\frac{q^2 x(1-x) + M_w^2}{\mu^2}\right) - \cdots\right]^{-1},\tag{6.61}$$

where $b_w = 11/24\pi^2$ and the ellipses denote the contributions of the fermion families. Clearly, $\widehat{d}_w(0) = \overline{g}_w^2(0)/M_w^2$, with

$$\overline{g}_w^2(0) = g_w^2(\mu)\left[1 + b_w g_w^2(\mu)\ln\left(\frac{M_w^2}{\mu^2}\right)\right]^{-1}.\tag{6.62}$$

Evidently, in the deep IR, the coupling freezes at a constant value; Fermi's constant is in fact determined as[7] $4\sqrt{2}G_F = \overline{g}_w^2(0)/M_w^2$.

This property of the freezing of the coupling can be reformulated in terms of what in the language of the effective field theories is referred to as *decoupling* [43]. At energies that are small compared to their masses, the particles appearing in the loops (in this case, the gauge bosons) cease to contribute to the running of the coupling. Possibly large logarithmic constants, e.g., $\ln(M_w^2/\mu^2)$, may be reabsorbed in the renormalized value of the coupling. Of course, the decoupling, as described earlier should not be misinterpreted to mean that the running coupling vanishes; instead, as already mentioned, it freezes at a constant, nonzero value. In other words, the decoupling does not imply that the theory becomes free (noninteracting) in the IR.

It would certainly be incorrect in such cases to insist on the perturbative prescription and simply factor out a $1/q^2$. Even though one is merely redistributing a given

---

[7] Note that in the case of QCD, the corresponding combination, $\overline{g}^2(0)/m^2(0)$, would be similar to a Nambu–Jona–Lasinio type of coupling [1]: at energies below the gluon mass m, the tree-level amplitude of four quarks starts looking a lot like that of a four-Fermi interaction.
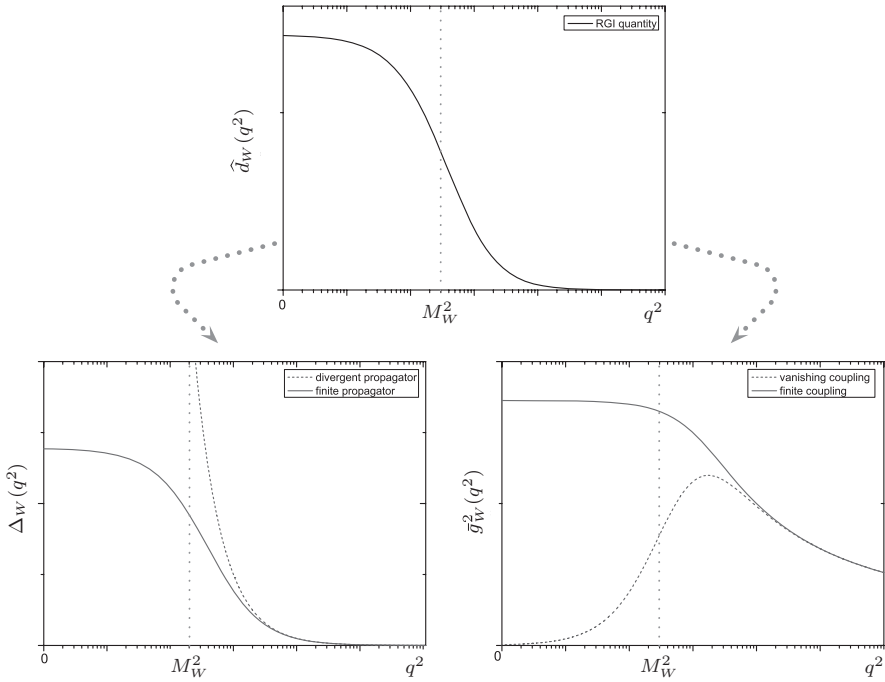
Figure 6.13. A sketch plot that shows how the same RG-invariant quantity in the presence of the mass scale M_w^2 can be decomposed in two different ways: one giving a divergent propagator and a vanishing coupling and the other, giving a finite propagator and a finite coupling.

function, namely, $\widehat{d}_w(q^2)$, into two pieces, factoring out $1/q^2$ deprives both of any physical meaning. Indeed, the effective coupling so defined would be given by the expression $\widetilde{g}_w^2(q^2) = q^2\widehat{d}_w(q^2)$, and so $\widetilde{g}_w^2(0) = 0$; evidently, one would be attempting to describe weak interactions in terms of a massless, IR-divergent, gauge-boson propagator and a vanishing effective coupling (see the dotted lines in Figure 6.13). Correspondingly, given that the gluon propagator is finite in the IR, if this latter (wrong) procedure were to be applied to QCD, it would furnish a completely unphysical coupling, namely, one that vanishes in the deep infrared, where QCD is expected to be (and is) strongly coupled.

After this long detour, let us return again to the basic equation (6.59). To actually determine the effective charge from $\widehat{d}(q^2)$, some additional information about the concrete running of $m^2(q^2)$ must be provided. The actual running of the mass may be determined dynamically through elaborate considerations that we will not present here. Instead, we will assume that $m^2(q^2)$ displays a power-law running, as shown by the early work of Lavelle [44] (see Chapter 2) and as has been independently confirmed within an entirely different formalism [45]. In Figure 6.14, we show the
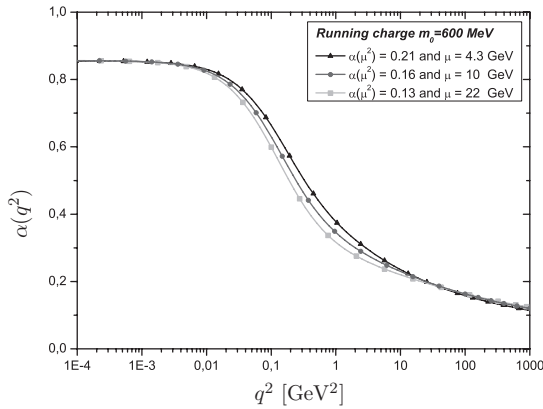
Figure 6.14. The effective charge $\alpha(q^2)$ obtained from the RG-invariant $\widehat{d}(q^2)$ using Eqs. (6.59) and (6.63) for a value of the effective gluon mass $m_0 = 600$ MeV.

effective charge, $\alpha = \overline{g}^2(q^2)/4\pi$, obtained from the $\widehat{d}(q^2)$ shown in Figure 6.14 (*left*) after using Eq. (6.59) with a running gluon mass of the form

$$m^2(q^2) = \frac{m_0^4}{q^2 + m_0^2}.$$ (6.63)

One observes the *freezing* of the coupling at a finite nonvanishing value,[8] which is a direct consequence of the appearance of the dynamical mass in the RG logarithm.

References

[1] C. Alexandrou, P. de Forcrand, and E. Follana, The gluon propagator without lattice Gribov copies, *Phys. Rev.* **D63** (2001) 094504.
[2] C. Alexandrou, P. de Forcrand, and E. Follana, The gluon propagator without lattice Gribov copies on a finer lattice, *Phys. Rev.* **D65** (2002) 114508.
[3] P. Boucaud et al., The infrared behaviour of the pure Yang-Mills Green functions, arXiv hep-ph/0507104.
[4] P. Boucaud et al., Short comment about the lattice gluon propagator at vanishing momentum, arXiv hep-lat/0602006.
[5] P. Boucaud, J. P. Leroy, A. Le Yaouanc, J. Micheli, O. Pene, and J. Rodriguez-Quintero, On the IR behaviour of the Landau-gauge ghost propagator, *JHEP* **0806** (2008) 099.
[6] P. O. Bowman, U. M. Heller, D. B. Leinweber, M. B. Parappilly, and A. G. Williams, Unquenched gluon propagator in Landau gauge, *Phys. Rev.* **D70** (2004) 034509.

---

[8] This means, in particular, that when quark masses are ignored, QCD becomes conformally invariant in the deep IR. The existence of such a conformal window has been advocated for certain applications of the AdS/CFT correspondence in QCD [46].

 [7] W. Kamleh, P. O. Bowman, D. B. Leinweber, A. G. Williams, and J. Zhang, Unquenching effects in the quark and gluon propagator, *Phys. Rev.* **D76** (2007) 094501.

 [8] A. Cucchieri, T. Mendes, O. Oliveira, and P. J. Silva, Just how different are *SU*(2) and *SU*(3) Landau-gauge propagators in the IR regime?, *Phys. Rev.* **D76** (2007) 114507.

 [9] O. Oliveira and P. J. Silva, Infrared gluon and ghost propagators from lattice QCD: Results from large asymmetric lattices, *Eur. Phys. J.* **A31** (2007) 790.

[10] O. Oliveira, P. J. Silva, E. M. Ilgenfritz, and A. Sternbeck, The gluon propagator from large asymmetric lattices, *PoS* **LAT2007** (2007) 323.

[11] O. Oliveira and P. J. Silva, The lattice infrared Landau gauge gluon propagator: The infinite volume limit, arXiv 0910.2897 [hep-lat].

[12] I. L. Bogolubsky, E. M. Ilgenfritz, M. Muller-Preussker, and A. Sternbeck, The Landau gauge gluon and ghost propagators in 4D *SU*(3) gluodynamics in large lattice volumes, *PoS* **LAT2007** (2007) 290.

[13] E. M. Ilgenfritz, M. Muller-Preussker, A. Sternbeck, A. Schiller, and I. L. Bogolubsky, Landau gauge gluon and ghost propagators from lattice QCD, *Braz. J. Phys.* **37** (2007) 193.

[14] I. L. Bogolubsky, V. G. Bornyakov, G. Burgio, E. M. Ilgenfritz, M. Müller-Preussker, P. Schemel, and V. K. Mitrjushkin, The Landau gauge gluon propagator: Gribov problem and finite-size effects, *PoS* **LAT2007** (2007) 318.

[15] I. L. Bogolubsky, E. M. Ilgenfritz, M. Müller-Preussker, and A. Sternbeck, Lattice gluodynamics computation of Landau gauge Green's functions in the deep infrared, *Phys. Lett.* **B676** (2009) 69.

[16] A. Cucchieri and T. Mendes, What's up with IR gluon and ghost propagators in Landau gauge? A puzzling answer from huge lattices, *PoS* **LAT2007** (2007) 297.

[17] A. Cucchieri and T. Mendes, Constraints on the IR behavior of the gluon propagator in Yang-Mills theories, *Phys. Rev. Lett.* **100** (2008) 241601.

[18] A. Cucchieri and T. Mendes, Landau-gauge propagators in Yang-Mills theories at beta = 0: Massive solution versus conformal scaling, *Phys. Rev.* **D81** (2010) 016005.

[19] A. Cucchieri and T. Mendes, Numerical test of the Gribov-Zwanziger scenario in Landau gauge, *PoS* **QCD-TNT09** (2010) 026.

[20] A. Sternbeck, L. von Smekal, D. B. Leinweber, and A. G. Williams, Comparing *SU*(2) to *SU*(3) gluodynamics on large lattices, *PoS* **LAT2007** (2007) 340.

[21] Y. B. Zhang, J. L. Ping, X. F. Lu, and H. S. Zong, Unquenched effects and quark mass dependence of lattice gluon propagator in infrared region, *Commun. Theor. Phys.* **50** (2008) 125.

[22] V. N. Gribov, Quantization of non-Abelian gauge theories, *Nucl. Phys.* **B139** (1978) 1.

[23] J. M. Cornwall, Dynamical mass generation in continuum QCD, *Phys. Rev.* **D26** (1982) 1453.

[24] D. Binosi and J. Papavassiliou, New Schwinger-Dyson equations for non-Abelian gauge theories, *JHEP* **0811** (2008) 063.

[25] D. Binosi and J. Papavassiliou, Gauge-invariant truncation scheme for the Schwinger-Dyson equations of QCD, *Phys. Rev.* **D77**(R) (2008) 061702.

[26] A. Cucchieri, T. Mendes, and A. Mihara, Numerical study of the ghost-gluon vertex in Landau gauge, *JHEP* **0412** (2004) 012.

[27] E. M. Ilgenfritz, M. Müller-Preussker, A. Sternbeck, and A. Schiller, Gauge-variant propagators and the running coupling from lattice QCD, arXiv hep-lat/0601027.

[28] A. C. Aguilar, D. Binosi, and J. Papavassiliou, Gluon and ghost propagators in the Landau gauge: Deriving lattice results from Schwinger-Dyson equations, *Phys. Rev.* **D78** (2008) 025010.

[29] T. Kugo and I. Ojima, Local covariant operator formalism of non-Abelian gauge theories and quark confinement problem, *Prog. Theor. Phys. Suppl.* **66** (1979) 1.

[30] T. Kugo, The universal renormalization factors Z(1)/Z(3) and color confinement condition in non-Abelian gauge theory, talk given at the International Symposium on BRS Symmetry on the Occasion of Its 20th Anniversary, Kyoto, Japan (1995).

[31] A. C. Aguilar, D. Binosi, J. Papavassiliou, and J. Rodriguez-Quintero, Non-perturbative comparison of QCD effective charges, *Phys. Rev.* **D80** (2009) 085018.

[32] A. C. Aguilar, D. Binosi, and J. Papavassiliou, Indirect determination of the Kugo-Ojima function from lattice data, *JHEP* **0911** (2009) 066.

[33] D. Zwanziger, Fundamental modular region, Boltzmann factor and area law in lattice gauge theory, *Nucl. Phys.* **B412** (1994) 657.

[34] A. Sternbeck, The infrared behavior of lattice QCD Green's functions, arXiv hep-lat/0609016, and references therein.

[35] M. Gell-Mann and F. E. Low, Quantum electrodynamics at small distances, *Phys. Rev.* **95** (1954) 1300.

[36] N. J. Watson, Universality of the pinch technique gauge boson self-energies, *Phys. Lett.* **B349** (1995) 155.

[37] J. Papavassiliou and A. Pilaftsis, Gauge invariance and unstable particles, *Phys. Rev. Lett.* **75** (1995) 3060.

[38] J. Papavassiliou and A. Pilaftsis, A gauge independent approach to resonant transition amplitudes, *Phys. Rev.* **D53** (1996) 2128.

[39] J. Papavassiliou and A. Pilaftsis, Gauge-invariant resummation formalism for two point correlation functions, *Phys. Rev.* **D54** (1996) 5315.

[40] N. J. Watson, The gauge-independent QCD effective charge, *Nucl. Phys.* **B494** (1997) 388.

[41] D. Binosi and J. Papavassiliou, The QCD effective charge to all orders, *Nucl. Phys. Proc. Suppl.* **121** (2003) 281.

[42] P. Boucaud et al., Artifacts and $<A^2>$ power corrections: Re-examining Z_ψ^2 and Z_v in the momentum-subtraction scheme, *Phys. Rev. D* **74** (2006) 034505.

[43] T. Appelquist and J. Carazzone, Infrared singularities and massive fields, *Phys. Rev.* **D11** (1975) 2856.

[44] M. Lavelle, Gauge invariant effective gluon mass from the operator product expansion, *Phys. Rev.* **D44** (1991) 26.

[45] D. Dudal, J. A. Gracey, S. P. Sorella, N. Vandersickel, and H. Verschelde, A refinement of the Gribov-Zwanziger approach in the Landau gauge: Infrared propagators in harmony with the lattice results, *Phys. Rev.* **D78** (2008) 065047.

[46] S. J. Brodsky and G. F. de Teramond, Light-front hadron dynamics and AdS/CFT correspondence, *Phys. Lett.* **B582** (2004) 211.